1	Iodine in metal organic frameworks at high pressure		
2			
3	Sergey S. Lobanov <sup>1,*</sup> , Kip Daly <sup>2</sup> , Alexander F. Goncharov <sup>3</sup> , Xiaojun Chan <sup>4</sup> , Lars Ehm <sup>1,5</sup> ,		
4	Taejin Kim <sup>4</sup> , John B. Parise <sup>1,2,6</sup>		
5			
6	<sup>1</sup> Department of Geosciences, Stony Brook University, Stony Brook, NY 11794, USA		
7	<sup>2</sup> Department of Chemistry, Stony Brook University, Stony Brook, NY 11794, USA		
8	<sup>3</sup> Geophysical Laboratory, Carnegie Institution of Washington, Washington, DC 20015, USA		
9	<sup>4</sup> Department of Materials Science and Chemical Engineering, Stony Brook University, Stony		
10	Brook, NY 11794, USA		
11	<sup>5</sup> Synchrotron Light Source-II, Brookhaven National Laboratory, PO Box 5000, Upton, NY		
12	11973, USA		
13	<sup>6</sup> Joint Photon Sciences Institute, Stony Brook University, Stony Brook, NY 11794, USA		
14			
15	Abstract		
16	Capture of highly-volatile radioactive iodine is a promising application of metal organic		
17	frameworks (MOFs), thanks to their high porosity with flexible chemical architecture.		
18	Specifically, strong charge-transfer binding of iodine to the framework enables efficient and		
19	selective iodine uptake as well as its long-term storage. As such, precise knowledge of the		
20	electronic structure of iodine is essential for a detailed modelling of the iodine sorption process,		
21	which will allow for rational design of iodophilic MOFs in the future. Here we probe the		
22	electronic structure of iodine in MOFs at variable iodineframework separation by Raman and		
23	optical absorption spectroscopy at high pressure (P). The electronic structure of iodine in the		
24	straight channels of SBMOF-1 ( $Ca$ - $sdb$ , $sdb = 4$ ,4 $^{\circ}$ - $sulfonyldibenzoate$ ) is modified irreversibly		
25	at $P > 3.4$ GPa by charge-transfer, marking a crossover in iodine chemical speciation. In contrast,		
26	iodine in the sinusoidal channels of SBMOF-3 (Cd-sdb) retains its molecular character up to at		
27	least 8.4 GPa. Such divergent high-pressure behavior of iodine in the MOFs with similar port		
28	size and chemistry suggests that the electronic structure of iodine is not fixed but adapts to		
29	channel geometry and strength of the iodineframework interaction. Our results exemplify that		
30	the topology of the sorption surface is another important factor governing the efficiency of iodine		
31	uptake by porous solids.		

# **Keywords:**

#### Introduction

Metal organic frameworks (MOFs) are synthetic porous solids with crystal structures made of two principal units: an organic linker and metal cluster. In constructing MOFs one has virtually endless flexibility to select linkers and metals to tailor frameworks for a specific application. As a result, thousands of MOFs are known to date with diverse physical and chemical properties that promise novel solutions for many grand challenges of the modern world, including selective gas sorption and storage. Of special interest is the use of MOFs for air purification owing to their high porosity and tunable chemical architectures which allow MOFs to outperform classical sorbents, such as zeolites and activated carbons, in the ability to trap toxic chemicals. One example is the use of MOFs for capturing radioactive iodine formed upon nuclear fuel fission, which has been notably challenging to immobilize due to its volatility. Rational design of iodophilic MOFs may enable next generation techniques for reprocessing of used nuclear fuel.

The iodine sorption capacity of many MOFs has been evaluated by exposing activated frameworks to iodine gas while monitoring the change in weight. <sup>4-10</sup> Several high surface area (>1500 m²/g) and large pore size (>10 Å) MOFs showed remarkable iodine uptake of more than 100 wt % and a packing density of ~2 g/cm³, surpassing the industrially used materials by a factor of 5-10. <sup>4-5, 8</sup> Surface area and pore size, however, appear to be of secondary importance as MFM-300 MOF series showed an even higher packing density (~3 g/cm³) within smaller (~8 Å) pores and the surface areas of ~1000-1200 m²/g. <sup>9</sup> Moreover, alternative porous compounds with much smaller surface areas (~10 m²/g) have comparable capacities <sup>11-12</sup>. Even nonporous compounds can host up to 20 wt % of I₂. <sup>13</sup>

Falaise, et al. <sup>6</sup> provided the first systematic insights into the primary factors governing iodine uptake by focusing on the MIL-53 MOF series with variable pore functionalization. MIL-53 decorated with electron-donating groups, such as NH<sub>2</sub>, showed the highest iodine uptake while its non-functionalized form performed the worst despite having a higher surface area (~1100 m<sup>2</sup>/g). Subsequent studies confirmed the importance of charge-transfer (CT) interactions for iodine adsorption by porous solids<sup>9, 12, 14-15</sup> The need for an electron-donating group in the

chemical structure of a MOF for its efficient iodine capture resonates with the increased iodine solubility in strong organic donors forming molecular CT complexes. <sup>16-17</sup> One can think of iodine adsorbed in a MOF as of an iodine-bearing molecular CT complex. The electronic structure of iodine in molecular complexes is perturbed by CT resulting in characteristic spectroscopic features that are not observed in pure iodine and its solvents. <sup>18</sup> Reliable spectroscopic signatures are now available to detect CT in iodine-bearing systems. <sup>16, 19-20</sup> Quantum-mechanical treatment of molecular CT complexes successfully reproduced these signatures and predicted that the donor-acceptor spatial separation, which can be controlled by pressure, governs the strength of their interaction. <sup>21</sup> This prediction found experimental confirmation in the limit of 0.5 GPa. <sup>16, 22</sup>

However, the electronic structure of iodine itself is very sensitive to external pressure. For example, molecular iodine dissociates to an atomic metal through an intermediate incommensurate phase where I-I bonds continuously vary in the 2.86-3.11 Å range.<sup>23</sup> Bond distances in the incommensurate phase are typical of polyiodides<sup>24</sup>, which themselves are energetically favored at high pressure due to its tendency to increase coordination.<sup>25</sup> Molecularorbital representation of bonding in polyiodides suggests their stability is due to CT interaction of neighboring iodine species (I<sub>2</sub>, I<sup>-</sup>, I<sub>3</sub><sup>-</sup>).<sup>24</sup> If polyiodides are present in MOFs, the CT interaction intrinsic to their bonding must compete with the iodine...framework binding CT interaction, and can affect iodine adsorption in the MOFs. High-pressure provides a unique window into this competition, as it allows isochemical variation of the iodine...framework and iodine...iodine separation within iodine-filled MOF, with implications for improving iodine uptake and selectivity. In addition, precise knowledge of the electronic structure of iodine species in MOFs is required for any thermodynamic modelling of their uptake kinetics and sorption selectivity. However, modelling work intended to locate iodine in powder diffraction studies, often assumes the presence of molecular I<sub>2</sub> only<sup>4-5</sup>, although the presence of polyiodide species in MOFs has been established by single crystal structural determination. <sup>26-27</sup> Spectroscopy provides a complementary tool, which is sensitive to the chemistry of the system and changes in iodine speciation in the pores.

Here we use Raman and electronic spectroscopy in combination with powder x-ray diffraction (PXRD) to probe the electronic structure of iodine in MOFs as a function of pressure. We compressed two structurally different MOFs (SBMOF-1 and SBMOF-3, SB for Stony Brook

University) that are based on *sdb* (*4,4*'-*sulfonyldibenzoate*) linker and an octahedrally-coordinated metal. Both SBMOF-1 (*Ca-sdb*) and SBMOF-3 (*Cd-sdb*) are similar in the pore size and its chemical decoration, but differ in having straight and sinusoidal channels, respectively (Fig. 1).<sup>28-29</sup> This diversity allows isolation of the effect of pore geometry on the donor-acceptor exchange between iodine species and the wall sites on the pore. Surprisingly, we find that at high pressure iodine in SBMOF-1 is perturbed by CT, while iodine in SBMOF-3 remains intact. The mechanism of the pressure-induced CT in the case of I@SBMOF-1 is complex and likely has donor contributions not only from the linker but also from neighboring iodine molecules, implying their aggregation into polyiodides.

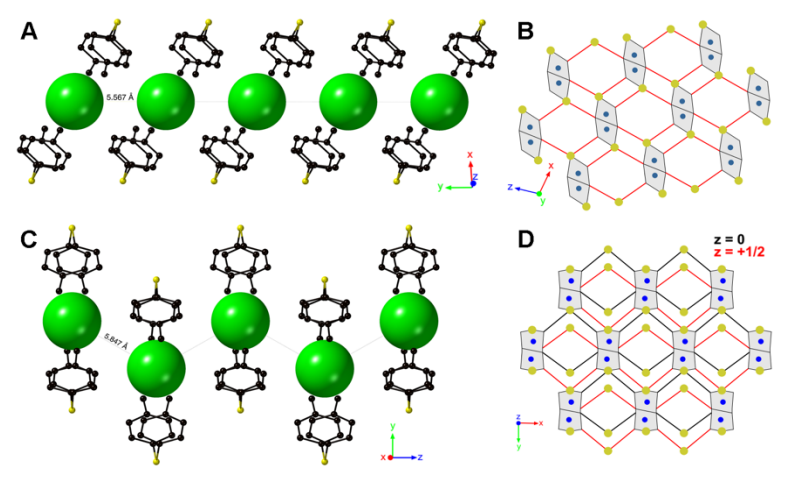


**Figure 1**. Straight channels in SBMOF-1(**A**) and sinusoidal in SBMOF-3 (**C**). Carbon atoms are black and sulfur is yellow. Oxygen, hydrogen, and calcium/cadmium atoms are omitted for clarity. Large green spheres depict iodine sorption sites. (**B**): 'Wine-rack' topology of SBMOF-1. Red wire is the *sdb* linker with all sulphonyl groups (yellow) bonded with Ca to form CaO<sub>6</sub>-octahedra (grey). All carboxyls also participate in CaO<sub>6</sub>-ocathedra and are not shown for clarity. (**D**): 'Wine-rack' topology of SBMOF-3. Black (z = 0) and red (z = 1/2) wire is the *sdb* linker with only half sulphonyl groups bonded with Cd to form CdO<sub>6</sub>-octahedra (grey). All carboxyls also participate in CdO<sub>6</sub> and are not shown for clarity.

#### Results

The absorption spectrum of  $I_2$  in inert organic solvents is dominated by bands at ~540 nm ( $^1\Sigma_{0+g} \rightarrow {}^3\Pi_{0+u}$ , B state) and ~515 nm ( $^1\Sigma_{0+g} \rightarrow {}^1\Pi_u$ , C state) $^{30-33}$ , which account for about 95 % of light extinction in the visible range. $^{33}$  Additionally, a band at ~680 nm ( $^1\Sigma_{0+g} \rightarrow {}^3\Pi_{1u}$ , A state) is dipole-allowed and may appear as a shoulder on the main absorption peak accounting for ~5 % of its intensity. In weakly interacting solvents, such as benzene, the B and C bands are blue-shifted to ~500 nm and their individual components are hard to resolve because of the overlap. $^{16}$ 

The single iodine sorption site in I@SBMOF-1 is in the vicinity of the phenyl ring with I<sub>2</sub> oriented nearly perpendicular to the plane of the organic group<sup>10</sup>. Such a conformation resembles that found in other iodine-benzene systems<sup>34</sup>; thus, I@SBMOF-1 is expected to bear spectroscopic similarities with iodine in benzene, a well-studied system at near ambient conditions. In view of it having the same linker, I@SBMOF-3 might be expected to show a similar spectroscopic behavior.

119

120

121

122

123

124

125

126

127

128

129

130

131

132

133

134

135

136

137

138

139

140

141

142

143

144

145

146

147

148

149

Figure 2A shows pressure-induced changes in the optical absorbance of I@SBMOF-1. At 0.3 GPa, the only major absorption feature is the asymmetric band centered at ~500 nm. Its assignment to the B and C states of I2 is straightforward. A-band is not resolved, due to the thin sample (~10-20 µm) as required for a DAC loading. Please note, that we did not solve for individual components of the overlapping B and C bands, which is adequate because these states are triplet and singlet states of the  $\pi_q^* \to \sigma_u^*$  transition.<sup>30</sup> The spectral position of this band is a convenient and sufficient way to characterize pressure-induced changes to the  $\pi_a^* - \sigma_u^*$  energy gap. In addition, it has been shown that the deconvolution of iodine absorption spectrum into the components is highly sensitive to the fitting model.<sup>32-33</sup> Below 400 nm and extending into the UV range is the absorption edge that is only present in iodine-loaded SBMOF-1. Iodine-free SBMOF-1 and I<sub>2</sub> are fairly transparent at 330-400 nm (Suppl. Fig. S1)<sup>31-33</sup>; hence, the assignment of the absorption edge in I@SBMOF-1 to the sdb-I2 CT band. 16, 35 The CT band in the spectra of I@SBMOF-1 is direct spectroscopic evidence of a donor-acceptor binding of iodine in the framework of SBMOF-1. Upon compression to 2.2 GPa, the position and width of the 500-nm band remain unchanged, as does the contribution of the sdb-I<sub>2</sub> CT band. At 3.4 GPa, the 500-nm band is slightly broadened and is less intense. At the same time, the CT band is intensified (red-shifted) abruptly and starts overlapping with the 500-nm band. Surprisingly, a very similar spectroscopic discontinuity is observed in iodine-free SBMOF-1 (Suppl. Fig. S1), indicating that the increased absorbance at < 400 nm in the iodine-loaded sample cannot be attributed solely to the intensification of the CT band and is at least partially related to a pressure-induced transformation in the MOF framework. At 4.8 GPa, the main absorption band is split into several components below and above the center at 500 nm. The splitting increases upon further compression and two components are clearly resolved at 7.5 GPa with centers at 455 and 600 nm, while the 500-nm peak is no longer present. In contrast to SBMOF-1, absorption spectra of SBMOF-3 do not change with pressure: the frequency and intensity of the

500-nm band as well as that of the CT absorption edge remain largely unchanged over the entire compression cycle to 7.5 GPa (Fig. 2B).

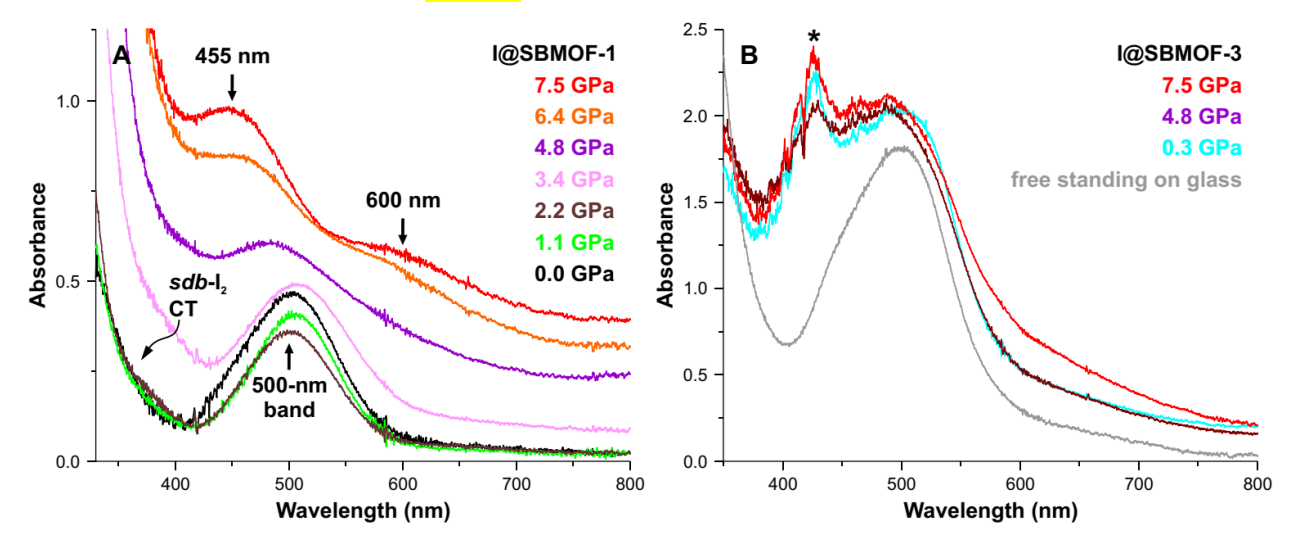


**Figure 2**. Absorption spectra of I@SBMOF-1 (**A**) and I@SBMOF-3 (**B**) measured upon compression to 7.5 GPa. Asterisk in (**B**) marks a spurious peak due to low intensity of the light source and poor sensitivity of the detector below 500 nm. For comparison, we show a spectrum of I@SBMOF-3 collected at a longer accumulation and outside diamond anvil cell (grey) that does not show the spurious peak.

Raman spectroscopy further confirms the different high-pressure behavior of iodine in the SBMOFs. Prior to compression, molecular iodine in I@SBMOF-1 gives rise to a narrow peak at 210 cm<sup>-1</sup> (labeled m-I<sub>2</sub>) (Fig. 3), characteristic of molecular (m) iodine in weak organic solvents.<sup>36</sup> No overtones are observed for this band as the Raman excitation wavelength (785 nm) provides a non-resonance scattering regime. The frequency of m-I<sub>2</sub> band increases continuously to 3.6 GPa ( $dv/dP = 4.8 \text{ cm}^{-1}/\text{GPa}$ ). The observed frequency shift is ~2.5 times larger than that observed in solid iodine (1.8 cm<sup>-1</sup>/GPa at P > 3 GPa);<sup>37</sup> thus, reveals an anomalously strong stiffening of the I-I bond in the straight channels of I@SBMOF-1 with pressure. Such a strong frequency shift suggests a rapid decrease of the I-I bond length and indicates that the bond is not perturbed by CT to the strongly antibonding  $\sigma_u^*$  orbital of I<sub>2</sub> as it would inevitably loosen the bond. At P > 3.6 GPa, the m-I<sub>2</sub> band cannot be clearly resolved. Instead, a new intense and broad peak centered at ~160 cm<sup>-1</sup> and a shoulder at ~190 cm<sup>-1</sup> appear in the Raman spectra. The new bands are about an order of magnitude more intense than the m-I<sub>2</sub> band and further intensify with compression. The width and position of the 160-190 cm<sup>-1</sup> feature are similar to that observed in iodine molecular complexes with strong organic donors, <sup>20</sup> where

the decreased frequency of I-I stretching is attributed to the CT interaction of the donor with the  $\sigma_u^*$  orbital of I<sub>2</sub>.<sup>38</sup> Interestingly, polyiodides containing diiodine perturbed by CT with an I<sub>n</sub><sup>-</sup> (n = 1, 3, 5, etc.) donor show indistinguishable Raman bands.<sup>38-39</sup> Following these previous studies, we assign the broad 160-190 cm<sup>-1</sup> to molecular iodine perturbed by CT interactions and label it p-I<sub>2</sub>. At 8.4 GPa, yet another new peak appears at ~110 cm<sup>-1</sup> and can be assigned to I<sub>3</sub><sup>-</sup> or I<sub>2</sub><sup>-</sup>.<sup>24,38-40</sup> At the highest pressure, p-I<sub>2</sub> band is ~100 times more intense than the m-I<sub>2</sub> band at 1 atm. In addition, a progression of overtones is observed for p-I<sub>2</sub>, suggesting a resonance-like enhancement of the higher order transitions, just as expected from the I@SBMOF-1 absorption spectra measured at P > 4 GPa which show strong absorption at the Raman excitation wavelength of 785 nm (Fig. 2A). The p-I<sub>2</sub> band is preserved on decompression to 1 atm, implying an irreversible character of the pressure-induced transformations in the electronic structure of iodine (Suppl. Fig. SX2).

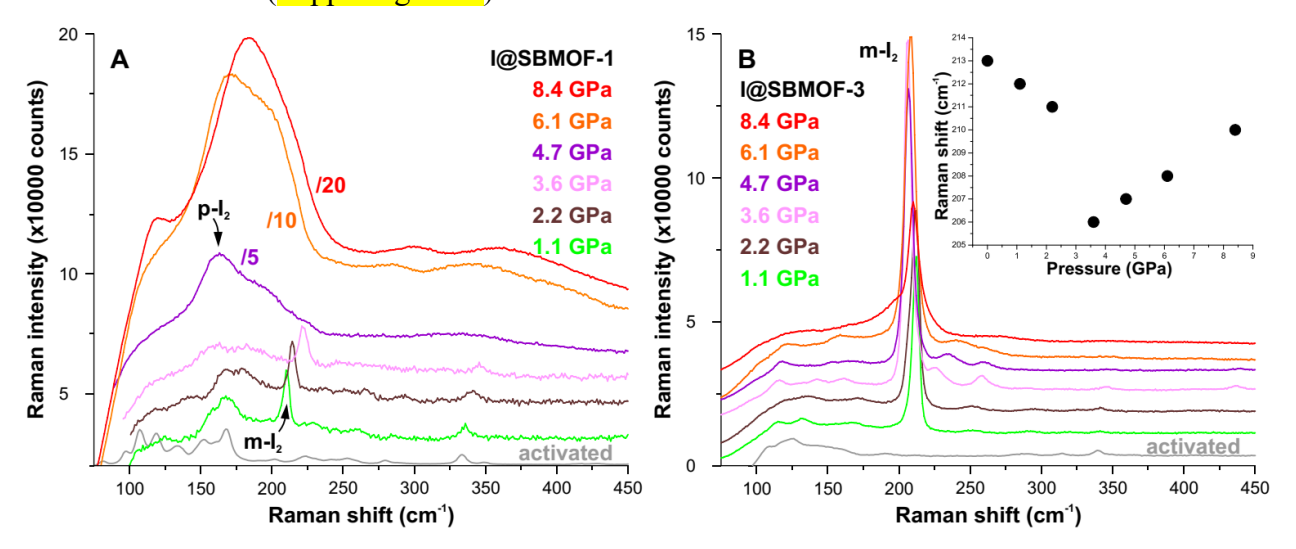


**Figure 3**. Raman spectra of I@SBMOF-1 (**A**) and I@SBMOF-3 (**B**) upon compression to 8.4 GPa collected using the 785-nm excitation. In (**A**): the intensity of the Raman spectra shown in purple, orange, and red has been divide by five, ten, and twenty, respectively. The spectra at 2.2, and 3.6 GPa are offset vertically by 1000 and 2000 counts for clarity. In (**B**): All Raman spectra of I@SBMOF-3 are offset vertically for clarity. The inset shows the Raman shift of m-I<sub>2</sub> in I@SBMOF-3 versus pressure. In (**A**) and (**B**): Raman spectra of activated SBMOF-1 and SBMOF-3 at 1 atm are shown in grey.

Raman spectra of I@SBMOF-3 collected in the same high-pressure run are all dominated by the m-I<sub>2</sub> peak (Fig. 3B). The frequency of m-I<sub>2</sub> decreases up to 3.6 GPa with an average slope of -2.4 cm<sup>-1</sup>/GPa. The negative frequency shift is quite unusual as it indicates loosening of the I-I bond with pressure. However, a very similar negative shift has been reported in solid I<sub>2</sub> (-2.1 cm<sup>-1</sup>)

 $^{1}$ /GPa) at pressures below ~3 GPa.  $^{37}$  Interestingly, the negative frequency shift of the I-I stretching vibration in I@SBMOF-3 is reversed at P > 3.6 GPa (Fig. 3B, inset). Again, a similar crossover in the sign of dv/dP has been observed in solid I<sub>2</sub> at  $P \sim 3$  GPa.  $^{37}$  The crossover indicates that the electronic structure of iodine in I@SBMOF-3 is governed by several competing factors such as a CT-induced loosening and pressure-induced stiffening of the bond; the latter apparently wins. The intensity of the m-I<sub>2</sub> band in the Raman spectra of I@SBMOF-3 increases steadily up to 6.1 GPa but is halved at 8.4 GPa due to the appearance of a low frequency shoulder at ~190-200 cm<sup>-1</sup>.

To gain insights into the compression mechanisms of iodine-loaded SBMOF-1 and SBMOF-3 we recorded PXRD patterns upon compression to ~3 GPa followed by decompression to 1 atm (Fig. 4). I@SBMOF-1 is prone to amorphization as evidenced by its broadened XRD peaks already at 1.1 GPa. Interestingly, the peak at  $\sim 1.2^{\circ} 2\Theta$ , which is a combination of  $10\overline{1}$  and 002 Bragg reflections, splits into these two components. Such splitting can only be attributed to framework flexing, which is enabled by the flexible C-S-C hinge in the center of the sdb linker and carbonyls on its ends, resulting in the increased  $\beta$  angle from its 1 atm value of ~100 to ~110° at 1.1 GPa. Framework flexing is characteristic of MOFs with compliant 'wine-rack' topologies<sup>41-46</sup> of which SBMOF-1 is a representative (Fig. 1B). Unfortunately, the corresponding powder XRD patterns are considerably broadened and do not allow for structure refinement at high pressure. The apparent pressure-induced disorder in I@SBMOF-1 is fully reversible upon decompression to 1 atm as revealed by PXRD and confirmed by Raman spectroscopy, unlike many other MOFs with irreversible pressure-induced transformations.<sup>46-47</sup> The reversibility not only suggests that the long range order is restored upon decompression, but also that pressure-induced changes in the short range atomic distribution are gradual and the overall framework topology is preserved at high pressure.

I@SBMOF-3 remains crystalline up to at least 3.4 GPa (Fig. 4B). The angular positions of the 110 and 220 reflections cross upon compression to 3.4 GPa, suggesting framework flexing along the a and b directions (Fig. 1D). Refining the I@SBMOF-3 unit cell at 3.4 GPa we obtain a 4.3 % reduction in a and 7.4 % increase in b. The apparent negative linear compressibility of I@SBMOF-3 is typical of compliant 'wine-rack' MOFs.  $^{41-46}$ 

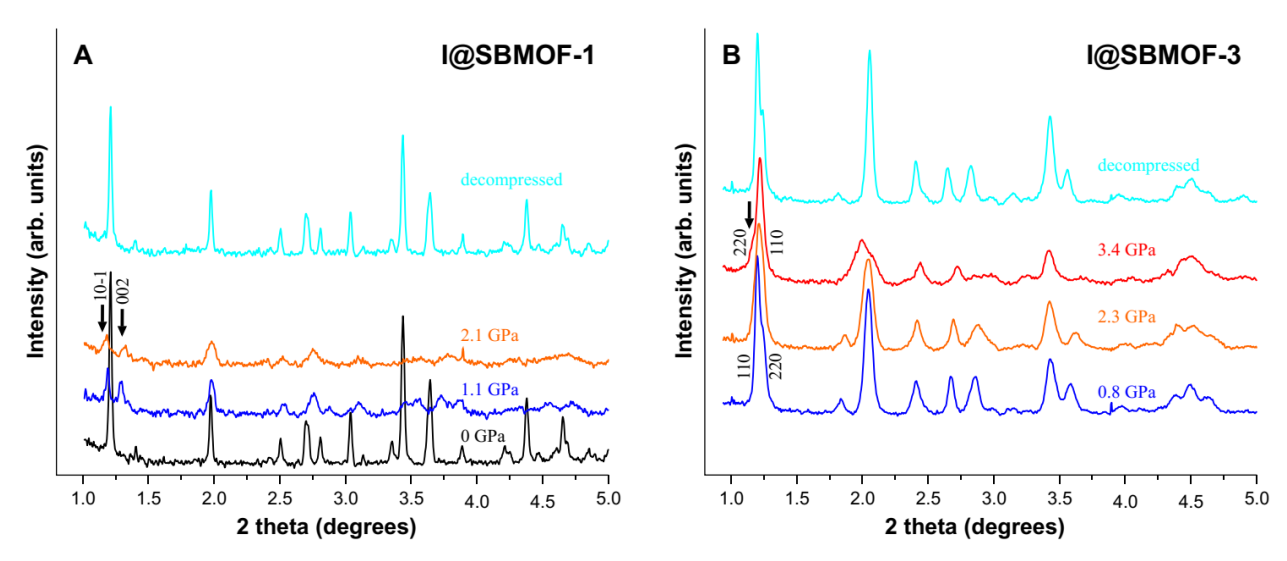


**Figure 4.** Powder x-ray diffraction patterns of I@SBMOF-1 (**A**) and I@SBMOF-3 (**B**) over a compression-decompression cycle. The x-ray wavelength is 0.2367 Å.

### **Discussion**

Spectroscopic data suggest a crossover in the electronic structure of iodine in I@SBMOF-1 at ~3.5 GPa. In contrast, the character of iodine in I@SBMOF-3 remains largely unchanged up to at least 8.4 GPa. Table 1 summarizes the main observations of this study.

Table 1. Summary of major observations in I@SBMOFs upon compression

Technique:	I@SBMOF-1	I@SBMOF-3
VIS	Fixed position of absorption edge @ P < 3.4	500-nm band persists in the studied P range
spectroscopy	GPa	
	Red-shift of absorption edge @ P > 3.4 GPa	
	500-nm band diminishing @ P > 3.4 GPa	
	New bands (455 and 600 nm) @ P > 3.4 GPa	
Raman	Strong positive <i>P</i> -shift of m-I <sub>2</sub> band	Negative <i>P</i> -shift of m-I <sub>2</sub> band @ $P < 3.6$ GPa
spectroscopy	m-I <sub>2</sub> band not resolved @ P > 3.6 GPa	Positive $P$ -shift of m-I <sub>2</sub> band @ P < 3.6 GPa
	Irreversible p-I <sub>2</sub> band @ P > 3.6 GPa	m-I <sub>2</sub> persists in the studied P range
	Resonance Raman for p-I <sub>2</sub>	
	New band at ~110 cm <sup>-1</sup> at 8.4 GPa	
PXRD	Reversible framework flexing	Reversible framework flexing
	Reversible amorphization @ P < 1 GPa	Crystalline up to at least 3.4 GPa

The frequency of I-I stretching in I@SBMOF-1 is  $\sim$ 160-170 cm<sup>-1</sup> at P = 3.6 GPa (p-I<sub>2</sub> band), well below its gas value ( $\sim$ 214 cm<sup>-1</sup>). Similar relatively low frequencies (150-180 cm<sup>-1</sup>)

of the I-I stretching vibration have been documented in the Raman spectra of polyiodides<sup>38-39, 48</sup> and iodine solutions in strong organic donors<sup>20, 39, 49</sup>. The reduced frequency is due to the increased electron density at the  $\sigma_u^*$  orbital of I<sub>2</sub> and is a fingerprint of strong donor-I<sub>2</sub> interaction, regardless of the donor kind.<sup>24, 39</sup> Two principal donor-acceptor scenarios can be proposed for I@SBMOF-1 at P > 3.6 GPa: (i) pressure-induced aggregation of iodine into polyiodide chains and (ii) pressure-enhanced CT between I<sub>2</sub> and phenyl of the *sdb* linker.

238

239

240

241

242

243

244

245

246

247

248

249

250

251

252

253

254

255

256

257

258

259

260

261

262

263

264

265

266

267

268

The disappearance of the 500-nm band  $(\pi_a^* \to \sigma_u^*)$  in the absorption spectra of I@SBMOF-1 at P > 3.4 GPa is consistent with these two principal types of donors as any CT increases the occupancy of the  $\sigma_{\nu}^*$  orbital. Likewise, both CT scenarios provide a qualitative explanation for the pressure-intensified (or red-shifted) absorption edge. For example, the CT band in the absorption spectra of benzene-I<sub>2</sub> complex intensifies and red-shifts continuously from 288 nm (1 atm) to 293 nm (0.2 GPa)<sup>50</sup>. On the other hand, electronic spectra of I<sub>3</sub><sup>-</sup>, the simplest polyiodide, have several broad absorption bands in the visible (centered at 565-590 and 440-460 nm) and UV range (< 350 nm)<sup>51-52</sup> as well as a distinct negative slope in the 350-800 nm range, just as the slope observed for I@SBMOF-1 at P > 4.8 GPa (Fig. 2A). Therefore, the newlyformed absorption bands at 600 and 455 nm may signal for polyiodide formation but their unique assignment is challenging. The energy difference between the new bands (~ 5300 cm<sup>-1</sup>) is characteristic of the spin-orbit splitting in I<sub>2</sub> (~5000 cm<sup>-1</sup>)<sup>33</sup>; thus, the new bands may be due to a new type of iodine species in I@SBMOF-1 at high pressure. Suppose an  $I_2^-$  anion ( $^2\Sigma_{1/2u}$  ground state) as a result of severe CT at 7.5 GPa. The lowest energy excited state of I<sub>2</sub>-would be split by spin-orbit coupling to the  ${}^2\Pi_{3/2g}$  and  ${}^2\Pi_{1/2g}$  states, both allowed by spectroscopic selection rules  $(\Delta\Omega=0,\pm 1)$ . Ab initio calculations of the ground and excited electronic states of  $I_2^-$  predicted a  $\sim$ 4700 cm<sup>-1</sup> gap between the  $^{2}\Pi_{3/2g} - ^{2}\Pi_{1/2g}$  states. <sup>53-54</sup> This gap is consistent with the observed ~5300 cm<sup>-1</sup> difference, while the spectral positions of the new bands appear at lower wavelengths than that predicted by theory (1030 and 710 nm) for an equilibrium I-I separation of ~3.1 Å. The I-I bond length is likely shorter at high pressure, which may account for the discrepancy in the excitation energy. Although the spectroscopic properties of I<sub>2</sub>- provide explanations for the new peaks at 600 and 455 nm, they do not help in discriminating between the proposed CT interactions.

The observed pressure-induced increase in  $\beta$  angle upon 'wine-rack' flexing is an efficient mechanism to overlap  $\pi$  electron density of the linker with diiodine molecular orbitals,

enhancing phenyl···I<sub>2</sub> CT interactions. However, one should expect exactly the same in I@SBMOF-3 as a consequence of its similar 'wine-rack' topology. Apparently, that is not the case as I@SBMOF-3 does not show any increase in the strength of donor···I<sub>2</sub> interaction and, as a consequence, the molecular character of I<sub>2</sub> is preserved up to at least 8.4 GPa. Why would two MOFs that are based on the same linker and exhibit similar pressure-induced pore flexing show such severe differences in their interaction with iodine?

The efficiency of any CT interaction depends critically not only on the donor-acceptor separation but also on their molecular orbital overlap. <sup>21</sup> Iodine in the straight channels of I@SBMOF-1 has the ability to interact with neighboring iodine species through a direct  $\sigma_u^* - \sigma_u^*$  overlap, which is achieved when I<sub>2</sub> molecular axes are aligned with the channel. Importantly, polyiodine building blocks ( $\Gamma$ , I<sub>3</sub>-, and I<sub>2</sub>) are prone to catenation and in many cases form linear or quasi-linear polyiodides structures. <sup>24,55</sup> In contrast, molecular orbital overlap in the sinusoidal channel of I@SBMOF-3 would be geometrically suppressed. The following spectroscopic and crystallographic arguments suggest that iodine in I@SBMOF-1 irreversibly forms 1D polyiodide chains.

The fixed spectral position of the absorption edge in I@SBMOF-1 at P < 3.4 GPa suggests that compression to 3.4 GPa does not enhance CT to iodine, which is also consistent with the nearly-fixed spectral position of the 500-nm band. <sup>16,50</sup> At P > 3.4 GPa, however, the abrupt red-shift of the absorption edge clearly signals for an enhanced CT. Shortening of the phenyl···I<sub>2</sub> distance with pressure, and therefore enhancement of their CT interaction, must be gradual upon 'wine-rack' flexing, inconsistent with the observed discontinuous position of the absorption edge. On the other hand, the nearly perpendicular orientation of I<sub>2</sub> to the phenyl ring in I@SBMOF-1 at 1 atm<sup>10</sup> precludes CT between neighboring I<sub>2</sub> molecules because of the lack of  $\sigma_u^* - \sigma_u^*$  overlap. Rotation of I<sub>2</sub> molecules upon 'wine-rack' flexing would produce an abrupt increase in I<sub>2</sub>-I<sub>2</sub> CT due to the  $\sigma_u^* - \sigma_u^*$  molecular orbital overlap along the straight channel.

In the crystal structure of I@SBMOF-1, the centers of neighboring  $I_2$  molecules are separated by 5.567 Å (at 1 atm) as templated by the unit cell repetition along the channel direction (Fig. 1A).<sup>10</sup> Upon pressure-induced 'wine-rack' flexing, rotation of discrete  $I_2$  units minimizes the repulsive interaction of its  $\pi_g^*$  (HOMO) with the  $\pi$  electron density of the linker. Iodine molecules aligned along the SBMOF-1 channel would be separated by ~2.9 Å, assuming initial I-I bond length (2.647 Å) is unaltered upon molecular rotation.<sup>10</sup> However, the  $I_2 \cdots I_2$ 

separation must be smaller than 2.9 Å because the CT interaction of neighboring I<sub>2</sub> molecules would inevitably loosen the intramolecular bond. Allowing for that, we obtain an extended 1D polyiodide chain in the I@SBMOF-1 channel with I-I bond of ~2.8 Å (Fig. 5). Such relatively long intramolecular I-I bond as well as the short I<sub>2</sub>···I<sub>2</sub> separation are characteristic of polyioides.<sup>24, 52, 55-56</sup> Raman spectroscopy provides an independent check on this qualitative scenario as the frequency of I-I stretching vibration correlates linearly with the I-I bond length<sup>38-39</sup>, predicting exactly 2.8 Å based on the frequency of p-I<sub>2</sub> (160 cm<sup>-1</sup> in decompressed I@SBMOF-1).

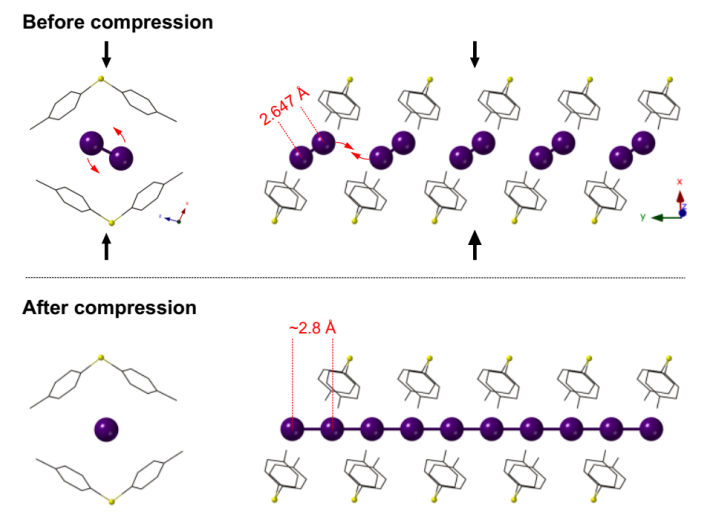


**Figure 5.** A spectroscopic model of the pressure-induced iodine polymerization in I@SBMOF-1. Black arrows depict the main flexing direction of the I@SBMOF-1 unit cell.

The framework of I@SBMOF-3 provides a larger dioiodine intermolecular distance of  $\sim$ 3.2 Å, outside the range of the I<sub>2</sub>···I<sub>2</sub> distances in polyiodides deposited in the Cambridge Structural Database. The sinusoidal channel of I@SBMOF-3 is also incommensurate with the formation of linear polyiodides. The very persistence of m-I<sub>2</sub> band in the Raman spectra of I@SBMOF-3 up to 8.4 GPa indicates that polyiodides are not formed in this MOF. As such, a sluggish CT to the  $\sigma_u^*$  orbital of I<sub>2</sub>, as signified by the negative frequency shift of the m-I<sub>2</sub> band at P < 3.6 GPa (Fig. 3B, inset), can only result from the iodine···phenyl interaction. This spectroscopic behavior can be viewed as a reference for a framework-to-iodine donor-acceptor exchange. Raman spectra of I@SBMOF-1 do not follow this model trend: the m-I<sub>2</sub> band in I@SBMOF-1 shows a rapid pressure-induced stiffening at P < 3.6 GPa, indicating that any CT interactions in this pressure range are not important. The abrupt disappearance of the m-I<sub>2</sub> peak

and a concurrent rise of the p- $I_2$  band at P > 3.6 GPa mark a crossover to iodine perturbed by CT. Given the similarities in pore size, chemistry, and pressure-flexing of I@SBMOF-1 and I@SBMOF-3, the sudden emergence of CT in I@SBMOF-1 is consistent with the formation of polyiodides at high pressure.

Finally, CT must affect not only the electron density and corresponding force constants of the acceptor but also the donor. For example, an upshift ( $\sim 10 \text{ cm}^{-1}$ ) of the C=C stretching frequency in carbon nanotubes has been observed upon iodine intercalation. <sup>57</sup> However, the Raman shift of the C=C stretching in I@SBMOF-1 and I@SBMOF-3 has a similar response to high pressure and does not show discontinuities at  $P \sim 3.5 \text{ GPa}$  (Suppl. Fig. S3). Therefore, the magnitude of iodine···phenyl CT interaction is comparable across the studied MOFs and shows little variation with pressure, consistent with the polyiodides formation.

#### Conclusions

Herein we have shown that the electronic structure of iodine shows a contrasting response to high pressure in the channels of two MOFs that are similar in their pore size, its chemistry and pressure-flexing. In the straight channel of I@SBMOF-1, iodine molecules are perturbed by CT interaction to form 1D chains along the channel. In contrast, iodine in I@SBMOF-3 appears to be shielded from CT interactions with neighboring iodine molecules by the sinusoidal shape of its channel. This work underscores the importance of channel topology of porous solids on the chemical state of the adsorbates with implications for an *ad hoc* design of MOFs.

### **Associated content**

This material is available free of charge via the Internet at http://pubs.acs.org. Supporting Information. Methods description, Absorption spectra of activated SBMOF-1 (Fig. S1), Raman spectra of I@SBMOF-1 over a full compression-decompression cycle (Fig. S2), Raman shift of the C=C symmetric stretching in I@SBMOF-1 and I@SBMOF-3 versus pressure (Fig. S3).

#### **Author information**

### **Corresponding author:**

\* E-mail: sergey.lobanov@stonybrook.edu; sergey.lobanov@gfz-potsdam.de

#### **Author contributions:**

355 The manuscript was written through contributions of all authors.

356

357

354

### Acknowledgement

- This research used beamline X-ray Powder Diffraction (XPD) beamline of the National
- 359 Synchrotron Light Source II, a U.S. Department of Energy (DOE) Office of Science User
- Facility operated for the DOE Office of Science by Brookhaven National Laboratory under
- 361 Contract No. DE-SC0012704. Work at the beamline was also supported by Hui Zhong of the
- Joint Photon Sciences Institute, an entity funded by the office of the provost, Stony Brook
- 363 University.

364 365 Reference

- 1. Furukawa, H.; Cordova, K. E.; O'Keeffe, M.; Yaghi, O. M., The chemistry and applications of metal-organic frameworks. *Science* **2013**, *341* (6149), 1230444.
- DeCoste, J. B.; Peterson, G. W., Metal-Organic Frameworks for Air Purification of Toxic Chemicals. *Chemical Reviews* **2014**, *114* (11), 5695-5727.
- 370 3. Soelberg, N. R.; Garn, T. G.; Greenhalgh, M. R.; Law, J. D.; Jubin, R.; Strachan, D. M.;
- 371 Thallapally, P. K., Radioactive Iodine and Krypton Control for Nuclear Fuel Reprocessing
- 372 Facilities. *Sci. Technol. Nucl. Install.* **2013**, *2013*, 1-12.
- 373 4. Sava, D. F.; Rodriguez, M. A.; Chapman, K. W.; Chupas, P. J.; Greathouse, J. A.; Crozier, P.
- 374 S.; Nenoff, T. M., Capture of volatile iodine, a gaseous fission product, by zeolitic imidazolate
- 375 framework-8. J. Am. Chem. Soc. **2011**, 133, 12398-12401.
- Sava, D. F.; Chapman, K. W.; Rodriguez, M. A.; Greathouse, J. A.; Crozier, P. S.; Zhao, H.
- 377 Y.; Chupas, P. J.; Nenoff, T. M., Competitive I<sub>2</sub> Sorption by Cu-BTC from Humid Gas Streams.
- 378 *Chem. Mater.* **2013**, *25*, 2591-2596.
- 379 6. Falaise, C.; Volkringer, C.; Facqueur, J.; Bousquet, T.; Gasnot, L.; Loiseau, T., Capture of
- iodine in highly stable metal-organic frameworks: a systematic study. *Chem. Commun.* **2013,** *49*
- 381 (87), 10320-10322.
- 382 7. Yao, R. X.; Cui, X.; Jia, X. X.; Zhang, F. Q.; Zhang, X. M., A Luminescent Zinc(II) Metal-
- Organic Framework (MOF) with Conjugated pi-Electron Ligand for High Iodine Capture and
- 384 Nitro-Explosive Detection. *Inorg. Chem.* **2016,** *55* (18), 9270-9275.
- 385 8. Li, B.; Dong, X.; Wang, H.; Ma, D.; Tan, K.; Jensen, S.; Deibert, B. J.; Butler, J.; Cure, J.; Shi,
- 386 Z.; Thonhauser, T.; Chabal, Y. J.; Han, Y.; Li, J., Capture of organic iodides from nuclear waste by
- metal-organic framework-based molecular traps. *Nature Communications* **2017**, *8* (1), 485.
- 388 9. Zhang, X. R.; da Silva, I.; Godfrey, H. G. W.; Callear, S. K.; Sapchenko, S. A.; Cheng, Y. Q.;
- 389 Vitorica-Yrezabal, I.; Frogley, M. D.; Cinque, G.; Tang, C. C.; Giacobbe, C.; Dejoie, C.; Rudic, S.;
- Ramirez-Cuesta, A. J.; Denecke, M. A.; Yang, S. H.; Schroder, M., Confinement of Iodine
- 391 Molecules into Triple-Helical Chains within Robust Metal-Organic Frameworks. J. Am. Chem.
- 392 *Soc.* **2017,** *139* (45), 16289-16296.

- 393 10. Banerjee, D.; Chen, X.; Lobanov, S. S.; Plonka, A. M.; Chan, X.; Daly, J. A.; Kim, T.;
- 394 Thallapally, P. K.; Parise, J. B., Iodine Adsorption in Metal Organic Frameworks in the Presence
- 395 of Humidity. ACS Appl. Mater. Interfaces 2018.
- 396 11. Ma, S. L.; Islam, S. M.; Shim, Y.; Gu, Q. Y.; Wang, P. L.; Li, H.; Sun, G. B.; Yang, X. J.;
- 397 Kanatzidis, M. G., Highly Efficient Iodine Capture by Layered Double Hydroxides Intercalated
- 398 with Polysulfides. *Chemistry of Materials* **2014**, *26* (24), 7114-7123.
- 399 12. Yan, Z.; Yuan, Y.; Tian, Y.; Zhang, D.; Zhu, G., Highly Efficient Enrichment of Volatile
- 400 Iodine by Charged Porous Aromatic Frameworks with Three Sorption Sites. *Angew. Chem., Int.*
- 401 *Ed. Engl.* **2015,** *54* (43), 12733-12737.
- 402 13. Jie, K. C.; Zhou, Y. J.; Li, E. R.; Li, Z. T.; Zhao, R.; Huang, F. H., Reversible Iodine Capture by
- 403 Nonporous Pillar[6] arene Crystals. J. Am. Chem. Soc. **2017**, 139 (43), 15320-15323.
- 404 14. Hughes, J. T.; Sava, D. F.; Nenoff, T. M.; Navrotsky, A., Thermochemical evidence for
- 405 strong iodine chemisorption by ZIF-8. *J. Am. Chem. Soc.* **2013,** *135* (44), 16256-16259.
- 406 15. Wang, Z.; Huang, Y.; Yang, J.; Li, Y. S.; Zhuang, Q. X.; Gu, J. L., The water-based synthesis
- 407 of chemically stable Zr-based MOFs using pyridine-containing ligands and their exceptionally
- 408 high adsorption capacity for iodine. *Dalton Trans.* **2017**, *46* (23), 7412-7420.
- 409 16. Benesi, H. A.; Hildebrand, J. H., A Spectrophotometric Investigation of the Interaction of
- 410 Iodine with Aromatic Hydrocarbons. J. Am. Chem. Soc. **1949**, 71 (8), 2703-2707.
- 411 17. Mulliken, R. S., Molecular Compounds and Their Spectra. III. The Interaction of Electron
- 412 Donors and Acceptors. J. Phys. Chem. **1952**, 56 (7), 801-822.
- 413 18. Mulliken, R. S., Structures of Complexes Formed by Halogen Molecules with Aromatic
- and with Oxygenated Solvents. J. Am. Chem. Soc. **1950**, 72 (1), 600-608.
- 415 19. Hastings, S. H.; Franklin, J. L.; Schiller, J. C.; Matsen, F. A., Molecular Complexes Involving
- 416 Iodine. J. Am. Chem. Soc. **1953**, 75 (12), 2900-2905.
- 417 20. Klaboe, P., Raman Spectra of Some Iodine Bromine and Iodine Monochloride Charge-
- 418 Transfer Complexes in Solution. J. Am. Chem. Soc. **1967**, 89 (15), 3667-3676.
- 419 21. Mulliken, R. S., Molecular Compounds and Their Spectra. II. J. Am. Chem. Soc. 1952, 74
- 420 (3), 811-824.
- 421 22. Sawamura, S.; Taniguchi, Y.; Suzuki, K., Effect of Pressure on Iodine Complexes. II.
- 422 Absorption-Spectra of the Charge-Transfer Bands with Diethyl Ether, Diethyl Sulfide, and
- Diethyl Selenide in Heptane. Bulletin of the Chemical Society of Japan 1979, 52 (2), 284-286.
- 424 23. Kenichi, T.; Kyoko, S.; Hiroshi, F.; Mitsuko, O., Modulated structure of solid iodine during
- its molecular dissociation under high pressure. *Nature* **2003**, *423* (6943), 971-974.
- 426 24. Svensson, P. H.; Kloo, L., Synthesis, structure, and bonding in polyiodide and metal
- 427 iodide-iodine systems. *Chemical Reviews* **2003**, *103* (5), 1649-1684.
- 428 25. Grochala, W.; Hoffmann, R.; Feng, J.; Ashcroft, N. W., The chemical imagination at work
- 429 in very tight places. Angew. Chem. Int. Ed. **2007**, 46 (20), 3620-3642.
- 430 26. Yin, Z.; Wang, Q. X.; Zeng, M. H., Iodine Release and Recovery, Influence of Polyiodide
- 431 Anions on Electrical Conductivity and Nonlinear Optical Activity in an Interdigitated and
- 432 Interpenetrated Bipillared-Bilayer Metal-Organic Framework. J. Am. Chem. Soc. 2012, 134 (10),
- 433 4857-4863.
- 434 27. Hu, X. L.; Sun, C. Y.; Qin, C.; Wang, X. L.; Wang, H. N.; Zhou, E. L.; Li, W. E.; Su, Z. M.,
- 435 Iodine-templated assembly of unprecedented 3d-4f metal-organic frameworks as
- photocatalysts for hydrogen generation. *Chem. Commun.* **2013**, *49* (34), 3564-3566.

- 437 28. Plonka, A. M.; Banerjee, D.; Woerner, W. R.; Zhang, Z. J.; Li, J.; Parise, J. B., Effect of
- 438 ligand geometry on selective gas-adsorption: the case of a microporous cadmium metal organic
- 439 framework with a V-shaped linker. *Chem Commun* **2013**, *49* (63), 7055-7057.
- 440 29. Banerjee, D.; Zhang, Z.; Plonka, A. M.; Li, J.; Parise, J. B., A Calcium Coordination
- 441 Framework Having Permanent Porosity and High CO<sub>2</sub>/N<sub>2</sub> Selectivity. Cryst. Growth Des. 2012,
- 442 *12* (5), 2162-2165.
- 443 30. Mulliken, R. S., Iodine Revisited. *Journal of Chemical Physics* **1971,** 55 (1), 288-&.
- 444 31. Tellinghuisen, J., Resolution of Visible-Infrared Absorption-Spectrum of I<sub>2</sub> into three
- 445 Contributing Transitions. *Journal of Chemical Physics* **1973**, *58* (7), 2821-2834.
- 446 32. Gray, R. I.; Luckett, K. M.; Tellinghuisen, J., Component analysis of the visible absorption
- spectra of I<sub>2</sub> and Br<sub>2</sub> in inert solvents: A critique of band decomposition by least-squares fitting.
- 448 J Phys Chem A **2001**, 105 (50), 11183-11191.
- 449 33. Tellinghuisen, J., Analysis of the Visible Absorption Spectrum of I<sub>2</sub> in Inert Solvents Using
- 450 a Physical Model. *J Phys Chem A* **2012**, *116* (1), 391-398.
- 451 34. Grozema, F. C.; Zijlstra, R. W. J.; Swart, M.; van Duijnen, P. T., Iodine-benzene charge-
- 452 transfer complex: Potential energy surface and transition probabilities studied at several levels
- 453 of theory. Int. J. Quantum. Chem. 1999, 75 (4-5), 709-723.
- 454 35. McConnell, H.; Ham, J. S.; Platt, J. R., Regularities in the Spectra of Molecular Complexes.
- 455 *Journal of Chemical Physics* **1953,** *21* (1), 66-70.
- 456 36. Kiefer, W.; Bernstein, H. J., Resonance Raman spectroscopic study on iodine in various
- organic solvents: Spectroscopic constants and halfband widths of the I2 vibration. J. Raman
- 458 *Spectrosc.* **1973,** *1* (5), 417-431.
- 459 37. Olijnyk, H.; Li, W.; Wokaun, A., High-Pressure Studies of Solid Iodine by Raman-
- 460 Spectroscopy. *Phys. Rev. B* **1994,** *50* (2), 712-716.
- 461 38. Deplano, P.; Devillanova, F. A.; Ferraro, J. R.; Mercuri, M. L.; Lippolis, V.; Trogu, E. F., Ft-
- 462 Raman Study on Charge-Transfer Polyiodide Complexes and Comparison with Resonance
- 463 Raman Results. *Appl Spectrosc* **1994**, *48* (10), 1236-1241.
- 464 39. Deplano, P.; Devillanova, F. A.; Ferraro, J. R.; Isaia, F.; Lippolis, V.; Mercuri, M. L., On the
- 465 Use of Raman-Spectroscopy in the Characterization of Iodine in Charge-Transfer Complexes.
- 466 Appl Spectrosc **1992**, 46 (11), 1625-1629.
- 467 40. Howard, W. F.; Andrews, L., Raman-Spectra of Alkali Metal-Iodine Matrix Reaction-
- 468 Products . Resonance Raman-Spectrum of Iodine Molecular Anion, I2<sup>-</sup>. J. Am. Chem. Soc. 1975,
- 469 *97* (11), 2956-2959.
- 470 41. Li, W.; Probert, M. R.; Kosa, M.; Bennett, T. D.; Thirumurugan, A.; Burwood, R. P.;
- 471 Parinello, M.; Howard, J. A. K.; Cheetham, A. K., Negative Linear Compressibility of a Metal-
- 472 Organic Framework. J. Am. Chem. Soc. **2012**, 134 (29), 11940-11943.
- 473 42. Ogborn, J. M.; Collings, I. E.; Moggach, S. A.; Thompson, A. L.; Goodwin, A. L.,
- 474 Supramolecular mechanics in a metal-organic framework. *Chem. Sci.* **2012,** *3* (10), 3011-3017.
- 475 43. Ortiz, A. U.; Boutin, A.; Fuchs, A. H.; Coudert, F. X., Metal-organic frameworks with wine-
- 476 rack motif: What determines their flexibility and elastic properties? Journal of Chemical Physics
- 477 **2013**, *138* (17).
- 478 44. Sarkisov, L.; Martin, R. L.; Haranczyk, M.; Smit, B., On the Flexibility of Metal-Organic
- 479 Frameworks. J. Am. Chem. Soc. **2014**, 136 (6), 2228-2231.

- 480 45. Cai, W. Z.; Katrusiak, A., Giant negative linear compression positively coupled to massive
- thermal expansion in a metal-organic framework. *Nature Communications* **2014,** 5.
- 482 46. McKellar, S. C.; Moggach, S. A., Structural studies of metal-organic frameworks under
- 483 high pressure. *Acta Cryst. B* **2015,** *71*, 587-607.
- 484 47. Spencer, E. C.; Kiran, M. S. R. N.; Li, W.; Ramamurty, U.; Ross, N. L.; Cheetham, A. K.,
- 485 Pressure-Induced Bond Rearrangement and Reversible Phase Transformation in a Metal-
- 486 Organic Framework. *Angew. Chem. Int. Ed.* **2014,** *53* (22), 5583-5586.
- 487 48. Ferraro, J. R.; Martin, K.; Furlani, A.; Russo, M. V., Vibrational Spectroscopy of Iodine-
- 488 Doped Poly(Phenyl)Acetylene. *Appl. Spectrosc.* **1984,** *38* (2), 267-270.
- 489 49. Tassaing, T.; Besnard, M., Ionization reaction in iodine/pyridine solutions: What can we
- learn from conductivity measurements, far-infrared spectroscopy, and Raman scattering? *J Phys*
- 491 *Chem A* **1997**, *101* (15), 2803-2808.
- 492 50. Ham, J., The Spectra of Iodine Solutions. II. The Effects of High Pressures Upon Iodine
- 493 Complexes. J. Am. Chem. Soc. **1954,** 76 (15), 3881-3885.
- 494 51. Gabes, W.; Stufkens, D. J., Electronic Absorption-Spectra of Symmetrical and
- 495 Asymmetrical Trihalide Ions. Spectrochim. Acta A 1974, A 30 (9), 1835-1841.
- 496 52. Mizuno, M.; Tanaka, J.; Harada, I., Electronic-Spectra and Structures of Polyiodide Chain
- 497 Complexes. J Phys Chem-Us 1981, 85 (13), 1789-1794.
- 498 53. Maslen, P. E.; Faeder, J.; Parson, R., Ab initio calculations of the ground and excited
- 499 states of I<sub>2</sub><sup>-</sup> and IC<sup>1</sup>. Chem. Phys. Lett. **1996**, 263 (1-2), 63-72.
- 500 54. Faeder, J.; Delaney, N.; Maslen, P. E.; Parson, R., Modeling structure and dynamics of
- solvated molecular ions: Photodissociation and recombination in I<sub>2</sub>-(CO(2)<sub>n</sub>. Chem. Phys. 1998,
- 502 *239* (1-3), 525-547.
- 503 55. Blake, A. J.; Devillanova, F. A.; Gould, R. O.; Li, W. S.; Lippolis, V.; Parsons, S.; Radek, C.;
- 504 Schroder, M., Template self-assembly of polyiodide networks. Chem Soc Rev 1998, 27 (3), 195-
- 505 205.
- 506 56. Kloo, L.; Rosdahl, J.; Svensson, P. H., On the intra- and intermolecular bonding in
- 507 polyiodides. Eur. J. Inorg. Chem. **2002**, (5), 1203-1209.
- 508 57. Grigorian, L.; Williams, K. A.; Fang, S.; Sumanasekera, G. U.; Loper, A. L.; Dickey, E. C.;
- Pennycook, S. J.; Eklund, P. C., Reversible intercalation of charged iodine chains into carbon
- 510 nanotube ropes. *Phys. Rev. Lett.* **1998**, *80* (25), 5560-5563.
- 511 58. Dewaele, A.; Torrent, M.; Loubeyre, P.; Mezouar, M., Compression curves of transition
- 512 metals in the Mbar range: Experiments and projector augmented-wave calculations. *Phys. Rev.*
- 513 B. **2008**, 78 (10).
- 59. Goncharov, A. F.; Beck, P.; Struzhkin, V. V.; Haugen, B. D.; Jacobsen, S. D., Thermal
- conductivity of lower-mantle minerals. *Physics of the Earth and Planetary Interiors* **2009,** 174 (1-
- 516 4), 24-32.
- 517 60. Goncharov, A. F.; Lobanov, S. S.; Tan, X.; Hohensee, G. T.; Cahill, D. G.; Lin, J. F.; Thomas,
- 518 S. M.; Okuchi, T.; Tomioka, N., Experimental study of thermal conductivity at high pressures:
- Implications for the deep Earth's interior. *Physics of the Earth and Planetary Interiors* **2015,** 247,
- 520 11-16.

### 523 SUPPLEMENTARY INFORMATION FOR 524 **Iodine** in metal organic frameworks at high pressure 525 526 Methods 527 Synthesis and iodine loading 528 Single crystals of SBMOF-1 and SBMOF-3 were synthesized under solvothermal conditions following the previously reported protocols. 10, 28-29 Subsequently, MOFs were 529 530 activated by heating in air at ~250 °C for ~12 h, and then exposed to dry iodine gas for 2 days in 531 a sealed chamber containing iodine crystals, similarly to our report on the iodine uptake by SBMOFs.<sup>10</sup> 532 Diamond anvil cell loadings 533 Almax plate DAC with diamond culets of 400 µm were used to generate high pressure. 534 535 Stainless steel foil with the initial thickness of 100 µm was indented to 40-60 µm by pressing on 536 the foil with the diamond anvils. A 250 µm hole was drilled in the center of the indentation to 537 serve as a sample chamber. Subsequently, the gasket was sonicated in ethanol for 30 min and positioned between the anvils. For all spectroscopic measurements high-quality single crystals of 538 539 I@SBMOF-1 and I@SBMOF-3 (and their activated forms) were positioned inside the sample chamber filled with silicon oil, serving as a non-penetrating pressure-transmitting medium. In 540 541 PXRD experiments, powders of the MOFs were loaded and the remaining sample chamber 542 volume was filled with silicon oil. All experiments were conducted at 300 K. Ruby was used as a pressure gauge.<sup>58</sup> 543 544 Raman spectroscopy Unpolarized Raman spectra were excited with a 785-nm XXX laser operating at ~2.5 545 546 mW. No laser-induced changes were evident at such relatively low laser power as confirmed by 547 a test run at 0.05 mW laser power. The choice of the 785-nm excitation is also important as 548 I@SBMOF-1 and I@SBMOF-3 have negligible absorbencies at this wavelength at 1 atm,

suppressing sample heating and possible light-induced changes. The laser was focused by a

Leica DM2500M microscope as part of the Renishaw inVia Raman system. Backscattered

radiation was collected by the same optical path, focused onto a 1200 line/mm diffraction

grating, and passed to an air-cooled CCD. Raman spectra were typically collected in the 50-2000

cm<sup>-1</sup> range with an overall exposure of 5-10 minutes. The spectra resolution was about 1 cm<sup>-1</sup>. In

549

550

551

552

553

addition, a 514-nm excitation of a He-Ne laser was used to excite ruby fluorescence, which was necessary for pressure measurements in the DAC (ruby fluorescence is at ~695 nm; thus cannot be excited by a 785-nm laser). All spectra were measured at room temperature.

## Electronic spectroscopy

Absorption spectra were collected by a custom-built microscope designed for optical measurements in a DAC.<sup>59</sup> Chromatic aberrations were minimized by all-reflective optics and the relatively small aberrations introduced by diamond anvils<sup>60</sup>, were accounted for by collecting a reference spectrum through the pressure medium. A fiber-coupled halogen-deuterium lamp (350-1100 nm) focused to a ~50  $\mu$ m spot on the sample served as a probe. The central portion of the transmitted radiation (~20  $\mu$ m) was projected onto the entrance slit of the Acton Research Corporation Spectra Pro 500-i spectrometer (300 grooves/mm) sensitive in the near-ultraviolet (UV), visible, and near-infrared (IR) range. All spectra were collected for 0.25 s at five different grating positions and then stitched together to produces a final spectrum. Samples absorbance was evaluates as:  $A(\nu) = -log_{10}(I_{sample} - I_{bckg})/(I_{reference} - I_{bckg})$ ), where  $I_{sample}$  is the intensity of light transmitted through the sample,  $I_{reference}$  is the intensity of light passed through the pressure medium, and  $I_{bckg}$  is the background reading. All spectra were collected at room temperature.

### Synchrotron powder x-ray diffraction (PXRD)

PXRD experiments were conducted at Beamline 28-ID-2 of NSLS-II. X-ray beam (52.38 keV) was collimated to ~0.3 x 0.2 mm<sup>2</sup> to minimize the contribution of gasket to the diffraction pattern. Sample-detector distance was calibrated by CeO<sub>2</sub>. Lars, please build on here.

### Polarized light microscopy

Polarization-dependent optical properties documented using an R40POL Fein Optic polarization microscope operating in transmission mode. Initial orientation of the polarization plane was confirmed by a standard (biotite) and then polarization was rotated to find most/least intense absorbance in the iodine-bearing MOFs. Once the most/least absorbance was achieved, polarization angle was documented. Accuracy of polarization angle measurements with respect to the most absorbing state was  $< 5^{\circ}$  as enabled by multiple measurements.

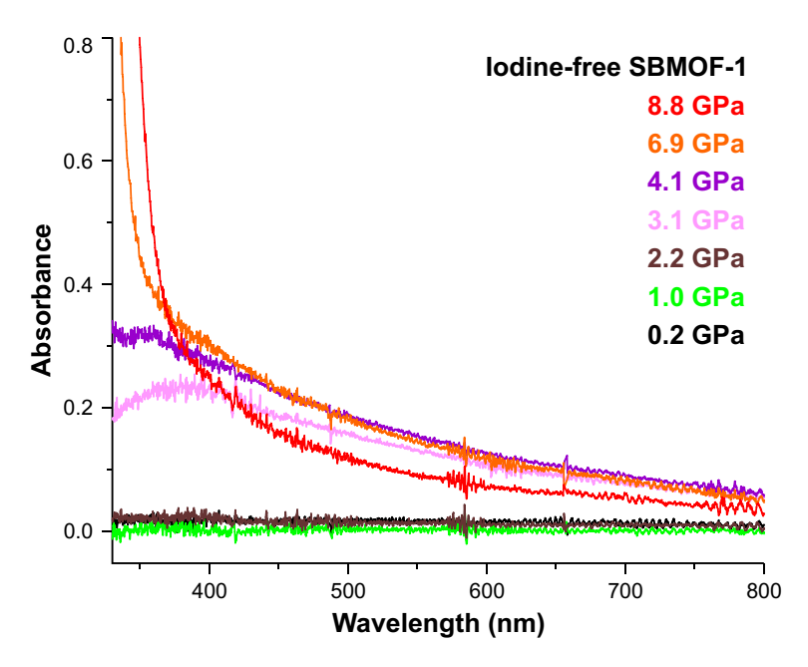
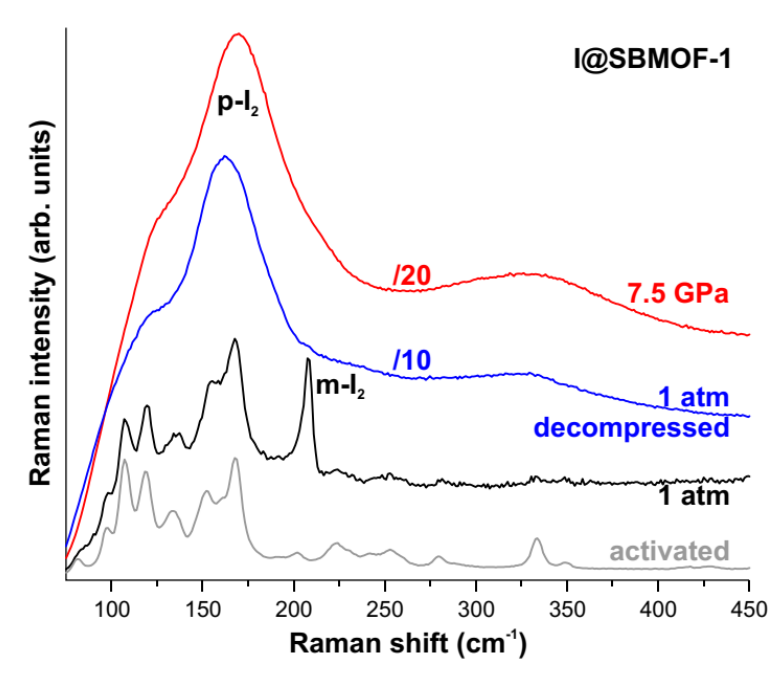
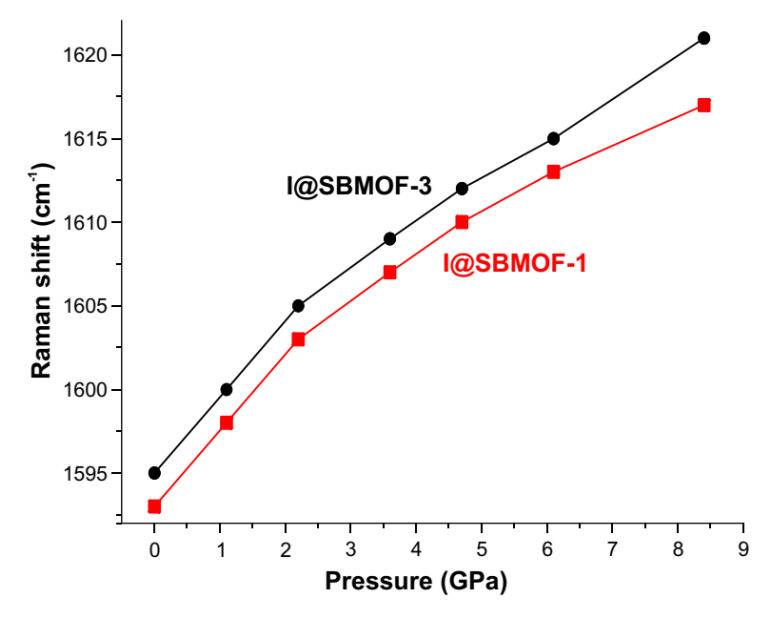


Figure S1. Absorption spectra of activated (iodine-free) SBMOF-1.



**Figure S2**. Representative Raman spectra of I@SBMOF-1 before compression (black), at 7.5 GPa (red), and decompressed to 1 atm (blue). Raman spectrum of iodine-free SBMOF-1 is shown in grey.



**Figure S3**. Raman shift of the C=C bond stretching in I@SBMOF-1 and I@SBMOF-3 as a function of pressure.